

Studies Towards a Scalable Synthesis of N-Acetyl-L-Fucosamine

by Ryan P. Conway

Ryan P. Conway

I hereby release this thesis to the public. I understand that this thesis will be made available from the OhioLINK ETD Center and the Maag Library Circulation Desk for public access. I also authorize the University or other individuals to make copies of this thesis as needed for scholarly research.

Submitted in Partial Fulfillment of the Requirements

for the Degree of

Signature:


Ryan P. Conway

Master of Science


8-7-07

Date

in the

Approvals:

Chemistry


Dr. Peter Norris
Thesis Advisor

Program

8-7-07

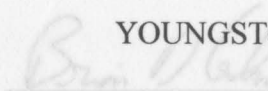
Date


Dr. John A. Jackson
Committee Member

8-7-07

Date


YOUNGSTOWN STATE UNIVERSITY


Dr. Brian D. Leskiw
Committee Member

August, 2007

8-7-07

Date


Dr. Peter J. Kasvinsky
Dean of Graduate Studies and Research

8/7/07
Date

Studies Towards a Scalable Synthesis of N-Acetyl-L-Fucosamine

Ryan P. Conway

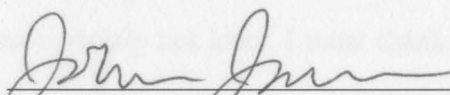
I hereby release this thesis to the public. I understand that this thesis will be made available from the OhioLINK ETD Center and the Maag Library Circulation Desk for public access. I also authorize the University or other individuals to make copies of this thesis as needed for scholarly research.

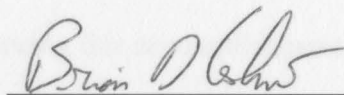
Signature:

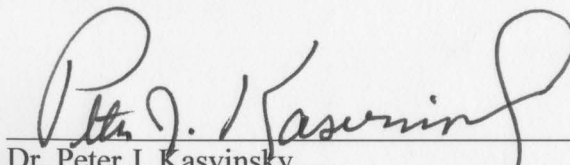

Ryan P. Conway 8-7-07
Date

Approvals:


Dr. Peter Norris 8-7-07
Thesis Advisor Date


Dr. John A. Jackson 8-7-07
Committee Member Date


Dr. Brian D. Leskiw 8-7-07
Committee Member Date


Dr. Peter J. Kasvinsky 8/7/07
Dean of Graduate Studies and Research Date

Thesis Abstract

The following describes two attempted syntheses of the rare sugar *N*-acetyl-L-fucosamine (L-FucNAc) from the inexpensive and readily available L-rhamnose. The syntheses will each involve a protection, oxidation, and reduction strategy in the inversion of the stereochemistry about two stereocenters in L-rhamnose, as well as the introduction of nitrogen at the C-2 position. *N*-Acetyl-L-fucosamine is one of three carbohydrate components of the capsular polysaccharide (CP) of *Staphylococcus aureus*, which protects the bacterium from the body's immune response. The termination of the CP may provide alternative therapies against *S. aureus* and possibly other pathogens.

My experience and your friendships have helped me more than you all know.

A very special thanks is reserved for my infinitely patient advisor Dr. Peter Norris whose guidance throughout both my undergraduate and graduate degrees has been paramount to my success. I cannot thank you enough, Doc.

Last but certainly not least, I must thank my family and especially my mother for all the support and love you've given me throughout my life; I could not have done this without you. This work is dedicated to my step-father Dave, who unfortunately passed away before seeing this accomplishment that he lovingly pushed me towards.

Acknowledgements

Title I would first like to thank the Youngstown State University, especially the Departments of Graduate Studies and Chemistry for giving me the opportunity to further my education by pursuing my Master's degree. I would also like to thank Dr. John Jackson and Dr. Brian Leskiw for graciously agreeing to be on my thesis committee and the feedback they've given me in my graduate research.

List of I am very grateful to have been a part of the Norris research group and for all of my colleagues and friends who have made my experience at YSU a truly enjoyable one. There are too many in the group to thank by name, but know I'll never forget this experience and your friendships have helped me more than you all know.

Introd A very special thanks is reserved for my infinitely patient advisor Dr. Peter Norris whose guidance throughout both my undergraduate and graduate degrees has been paramount to my success. I cannot thank you enough, Doc.

Conclu Last but certainly not least, I must thank my family and especially my mother for all the support and love you've given me throughout my life; I could not have done this without you. This work is dedicated to my step-father Dave, who unfortunately passed away before seeing this accomplishment that he lovingly pushed me towards.

Appendix B

152

Table of Contents

Title Page	Enzymatic conversion of D-GlcNAc-1-phosphate to UDP-L-FucNAc	i
Signature Page		ii
Thesis Abstract	First synthetic strategy from L-rhamnose to a protected FucNAc	iii
Acknowledgements	Isolation of the C-4 hydroxyl from L-rhamnose	iv
Table of Contents	Proposed trans-acetylation mechanism of 14 to 15	v
List of Schemes	Proposed mechanism of MOB ether cleavage of 16	vi
List of Equations	Proposed mechanism of pivaloyl cleavage and formation of 23	vi
List of Figures		vii
List of Tables		xi
Introduction	1-FucNAc	15
Statement of Problem	Isolation of the anomeric hydroxyl as a 4-methoxyphenol glycoside	13
Results and Discussion		14
Conclusion		43
Experimental		44
References		78
Appendix A		81
Equation 1:	Attempted Swern oxidation of 9	17
Equation 2:	Attempted biphasic $K_2Cr_2O_7$ oxidation of 9	17
Equation 3:	Formation of ketone 10 via PCC oxidation	18
Equation 4:	Attempted catalytic PCC oxidation of 9	19
Equation 5:	Dess-Martin oxidation of 9 to ketone 10	19
Equation 6:	Stereoselective reduction of ketone 10	20
Equation 7:	Protection of 11 by acetylation	21

List of Schemes	acid-catalyzed deprotection of 13	21
Scheme 1:	Enzymatic conversion of D-GlcNAc-1-phosphate to UDP-L-FucNAc	23
Equation 10:	<i>p</i> -Toluenesulfonic acid-catalyzed hydrolysis of 16 to 17	25
Scheme 2:	First synthetic strategy from L-rhamnose to a protected L-FucNAc	14
Equation 11:	L-FucNAc protection of 11 via Williamson ether synthesis	27
Scheme 3:	Isolation of the C-4 hydroxyl from L-rhamnose	15
Equation 12:	TFA-catalyzed hydrolysis of 18	27
Scheme 4:	Proposed trans-acetylation mechanism of 14 to 15	22
Equation 13:	Selective protection of 19 as a pivaloyl ester	28
Scheme 5:	Proposed mechanism of MOB ether cleavage of 16	25
Equation 14:	Attempted C-2 azidation of 20	29
Scheme 6:	Proposed mechanism of pivaloyl cleavage and formation of 23	30
Equation 15:	Formation of 25 through benzoylation	30
Scheme 7:	Formation of the C-2 oxime 25	31
Scheme 8:	Second synthetic strategy from L-rhamnose to a protected L-FucNAc	34
Equation 18:	Attempted NaBH ₄ CN reduction of 26	34
Scheme 9:	Protection of the anomeric hydroxyl as a 4-methoxyphenol glycoside	36
Equation 19:	Formation of 32 via Williamson ether synthesis	36
Scheme 10:	Isolation of C-4 of the 4-methoxyphenol glycoside	37
Scheme 11:	Inversion of the C-4 stereocenter	39
List of Figures	Hydrogen bonding effects of modification of cell wall subunits	15
List of Equations	Examples of carbohydrates in pharmaceuticals	15
Equation 1:	Attempted Swern oxidation of 9 and ketose	17
Equation 2:	Attempted biphasic K ₂ Cr ₂ O ₇ oxidation of 9	17
Equation 3:	Formation of ketone 10 via PCC oxidation	18
Equation 4:	Attempted catalytic PCC oxidation of 9 of <i>Staphylococcus aureus</i> in hospitals (closed symbols) and the community	19
Equation 5:	Dess-Martin oxidation of 9 to ketone 10	19
Equation 6:	Stereoselective reduction of ketone 10	20
Figure 6:	Hydrogen bonding effects of modification of cell wall subunits	
Equation 7:	Protection of 11 by acetylation	21

Equation 8:	Acid-catalyzed deprotection of 13	21
Equation 9:	MOB ether protection of 11 via Williamson ether synthesis	23
Equation 10:	<i>p</i> -Toluenesulfonic acid-catalyzed hydrolysis of 16 to 17	25
Equation 11:	Methyl ether protection of 11 via Williamson ether synthesis	27
Equation 12:	TFA-catalyzed hydrolysis of 18	27
Equation 13:	Selective protection of 19 as a pivaloyl ester	28
Equation 14:	Attempted C-2 azidation of 20	29
Equation 15:	Activation of 25 through benzylation	32
Equation 16:	Attempted BH ₃ reduction of 26	33
Equation 17:	Attempted NaBH ₄ reduction of 26	34
Equation 18:	Attempted NaBH ₃ CN reduction of 26	34
Equation 19:	Protection of 32 via Williamson ether synthesis	40
Equation 20:	Deprotection of the anomeric hydroxyl of 33	42
Figure 19:	Mass spectrum of 8	84
List of Figures	100 MHz ¹ H NMR spectrum of 9	85
Figure 1:	Examples of carbohydrates in pharmaceuticals	16
Figure 2:	Examples of a six-carbon aldose and ketose	27
Figure 3:	Five forms of D-glucose	38
Figure 4:	Differences in starch and cellulose linkages	59
Figure 5:	Increase in methicillin-resistant strains of <i>Staphylococcus aureus</i> in hospitals (closed symbols) and the community (open symbols)	90
Figure 26:	IR spectrum of 11	61
Figure 27:	100 MHz ¹³ C NMR spectrum of 11	92
Figure 6:	Hydrogen bonding effects of modification of cell wall subunits to vancomycin binding affinity	83

Figure 7:	<i>S. aureus</i> glycoalyx types 5 and 8	9
Figure 8:	X-Ray crystal structure of protected 2,6-dideoxy- <i>N</i> -acetyl-L-talosamine	95
Figure 9:	X-Ray crystal structures of 2,6-dideoxy- <i>N</i> -acetyl-L-fucosamine (left) and its protected 2-azidodeoxy derivative right)	12
Figure 10:	Orbital overlapping effects on α - and β -anomers	15
Figure 11:	X-Ray crystal structure of 9	16
Figure 12:	X-Ray crystal structure of 16	24
Figure 13:	X-Ray crystal structure of 17	26
Figure 14:	X-Ray crystal structure of 26	32
Figure 15:	X-Ray crystal structure of 29	38
Figure 16:	X-Ray crystal structure of 33	41
Figure 17:	400 MHz ^1H NMR spectrum of 8	82
Figure 18:	100 MHz ^{13}C NMR spectrum of 8	83
Figure 19:	Mass spectrum of 8	84
Figure 20:	400 MHz ^1H NMR spectrum of 9	85
Figure 21:	100 MHz ^{13}C NMR spectrum of 9	86
Figure 22:	Mass spectrum of 9	87
Figure 23:	400 MHz ^1H NMR spectrum of 10	88
Figure 24:	100 MHz ^{13}C NMR spectrum of 10	89
Figure 25:	Mass spectrum of 10	90
Figure 26:	400 MHz ^1H NMR spectrum of 11	91
Figure 27:	100 MHz ^{13}C NMR spectrum of 11	92
Figure 28:	Mass spectrum of 11	93

Figure 29:	400 MHz ^1H NMR spectrum of 12	94
Figure 30:	Mass spectrum of 12	95
Figure 31:	400 MHz ^1H NMR spectrum of 13	96
Figure 32:	Mass spectrum of 13	97
Figure 33:	100 MHz ^1H NMR spectrum of 14	98
Figure 34:	Mass spectrum of 14	99
Figure 35:	400 MHz ^1H NMR spectrum of 15	100
Figure 36:	Mass spectrum of 15	101
Figure 37:	400 MHz ^1H NMR spectrum of 16	102
Figure 38:	Mass spectrum of 16	103
Figure 39:	400 MHz ^1H NMR spectrum of 17	104
Figure 40:	Mass spectrum of 17	105
Figure 41:	400 MHz ^1H NMR spectrum of 18	106
Figure 42:	100 MHz ^{13}C NMR spectrum of 18	107
Figure 43:	Mass spectrum of 18	108
Figure 44:	400 MHz ^1H NMR spectrum of 19	109
Figure 45:	100 MHz ^{13}C NMR spectrum of 19	110
Figure 46:	Mass spectrum of 19	111
Figure 47:	400 MHz ^1H NMR spectrum of 20	112
Figure 48:	100 MHz ^{13}C NMR spectrum of 20	113
Figure 49:	Mass spectrum of 20	114
Figure 50:	400 MHz ^1H NMR spectrum of 21	115
Figure 51:	Mass spectrum of 21	116

Figure 52:	400 MHz ^1H NMR spectrum of 22	117
Figure 53:	Mass spectrum of 22	118
Figure 54:	400 MHz ^1H NMR spectrum of 23	119
Figure 55:	400 MHz ^1H NMR spectrum of 24	120
Figure 56:	100 MHz ^{13}C NMR spectrum of 24	121
Figure 57:	Mass spectrum of 24	122
Figure 58:	400 MHz ^1H NMR spectrum of 25	123
Figure 59:	100 MHz ^{13}C NMR spectrum of 25	124
Figure 60:	Mass spectrum of 25	125
Figure 61:	400 MHz ^1H NMR spectrum of 26	126
Figure 62:	100 MHz ^{13}C NMR spectrum of 26	127
Figure 63:	Mass spectrum of 26	128
Figure 64:	400 MHz ^1H NMR spectrum of 27	129
Figure 65:	100 MHz ^{13}C NMR spectrum of 27	130
Figure 66:	Mass spectrum of 27	131
Figure 67:	400 MHz ^1H NMR spectrum of 28	132
Figure 68:	100 MHz ^{13}C NMR spectrum of 28	133
Figure 69:	Mass spectrum of 28	134
Figure 70:	400 MHz ^1H NMR spectrum of 29	135
Figure 71:	100 MHz ^{13}C NMR spectrum of 29	136
Figure 72:	Mass spectrum of 29	137
Figure 73:	400 MHz ^1H NMR spectrum of 30	138
Figure 74:	100 MHz ^{13}C spectrum of 30	139
Table 3:	Band lengths [\AA] and angles [deg] for 9	157

Figure 75:	Mass spectrum of 30	140
Figure 76:	400 MHz ^1H NMR spectrum of 31	141
Figure 77:	100 MHz ^{13}C NMR spectrum of 31	142
Figure 78:	Mass spectrum of 31	143
Figure 79:	400 MHz ^1H NMR spectrum of 32	144
Figure 80:	100 MHz ^{13}C NMR spectrum of 32	145
Figure 81:	Mass spectrum of 32	146
Figure 82:	400 MHz ^1H NMR spectrum of 33	147
Figure 83:	100 MHz ^{13}C NMR spectrum of 33	148
Figure 84:	Mass spectrum of 33	149
Figure 85:	400 MHz ^1H NMR spectrum of 34	150
Figure 86:	Mass spectrum of 34	151
Figure 87:	X-Ray crystal structure of 9	153
Figure 88:	X-Ray crystal structure of 16	162
Figure 89:	X-Ray crystal structure of 17	173
Figure 90:	X-Ray crystal structure of 26	188
Figure 91:	X-Ray crystal structure of 29	208
Figure 92:	X-Ray crystal structure of 33	230
List of Tables		
Table 1:	Crystal data and structure refinement for 9	154
Table 2:	Atomic coordinates [$\times 10^4$] and equivalent isotropic displacement parameters [$\text{\AA}^2 \times 10^3$] for 9	156
Table 3:	Bond lengths [\AA] and angles [deg] for 9	157

Table 4:	Anisotropic displacement parameters [$\text{\AA}^2 \times 10^3$] for 9	160
Table 5:	Hydrogen coordinates ($\times 10^4$) and isotropic displacement parameters ($\text{\AA}^2 \times 10^3$) for 9	161
Table 6:	Crystal data and structure refinement for 16	163
Table 7:	Atomic coordinates [$\times 10^4$] and equivalent isotropic displacement parameters [$\text{\AA}^2 \times 10^3$] for 16	165
Table 8:	Bond lengths [\AA] and angles [deg] for 16	166
Table 9:	Anisotropic displacement parameters [$\text{\AA}^2 \times 10^3$] for 16	170
Table 10:	Hydrogen coordinates ($\times 10^4$) and isotropic displacement parameters ($\text{\AA}^2 \times 10^3$) for 16	171
Table 11:	Crystal data and structure refinement for 17	174
Table 12:	Atomic coordinates [$\times 10^4$] and equivalent isotropic displacement parameters [$\text{\AA}^2 \times 10^3$] for 17	176
Table 13:	Bond lengths [\AA] and angles [deg] for 17	178
Table 14:	Anisotropic displacement parameters [$\text{\AA}^2 \times 10^3$] for 17	183
Table 15:	Hydrogen coordinates ($\times 10^4$) and isotropic displacement parameters ($\text{\AA}^2 \times 10^3$) for 17	184
Table 16:	Torsion angles [deg] for 17	185
Table 17:	Hydrogen bonds for 17 [\AA and deg]	187
Table 18:	Crystal data and structure refinement for 26	189
Table 19:	Atomic coordinates [$\times 10^4$] and equivalent isotropic displacement parameters [$\text{\AA}^2 \times 10^3$] for 26	191
Table 20:	Bond lengths [\AA] and angles [deg] for 26	193
Table 21:	Anisotropic displacement parameters [$\text{\AA}^2 \times 10^3$] for 26	201
Table 22:	Hydrogen coordinates ($\times 10^4$) and isotropic displacement parameters ($\text{\AA}^2 \times 10^3$) for 26	203

Introduction

Carbohydrate Background

Emil Fischer's work in the late 1800s on carbohydrates, or sugars, was the first step in discovering a vastly important field of chemistry. His work on simple sugars would lead to the basic understanding of these molecules, which are now known to be vital to life. Carbohydrates are the most abundant organic molecules found in nature. They not only act as a primary energy source, but are also incorporated into the primary building blocks of all life, DNA. In recent years, carbohydrates have become the target of a great deal of research both academic and industrial. Derivatives of these molecules have been used in the pharmaceutical industry as antibiotics such as streptomycin,¹ and in anti-tumor agents such as sialyl-Tn (sTn) (Figure 1).²

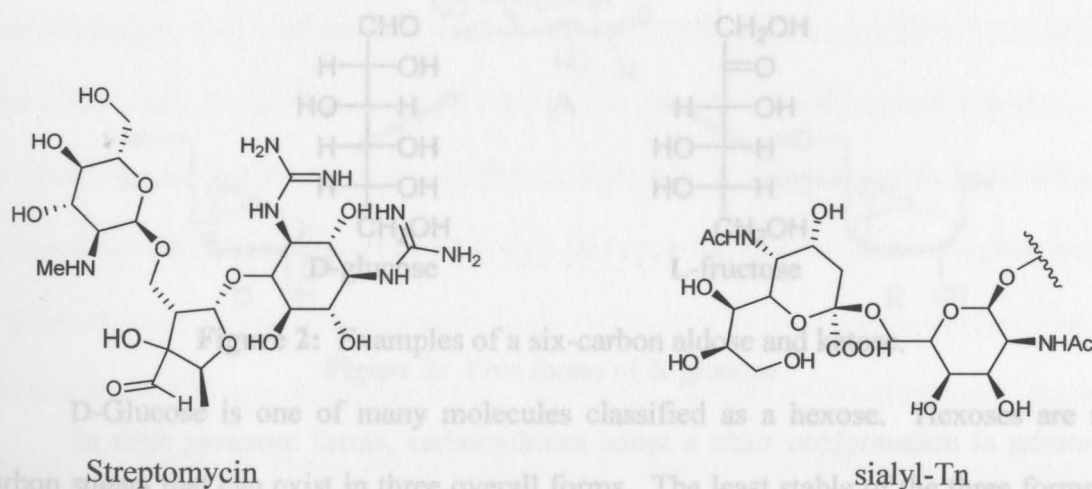


Figure 1: Examples of carbohydrates in pharmaceuticals.

The basic unit of a carbohydrate is known as a monosaccharide. The majority of monosaccharides are between three and six carbons in length and contain multiple hydroxyl groups. Most monosaccharides contain an aldehyde or ketone, many remaining consistent with the general equation of a simple sugar, $(\text{CH}_2\text{O})_n$. The aldoses contain an

aldehyde group at one end of the carbon chain, often a primary alcohol at the other end, and a varying number of carbon atoms attached to secondary alcohols. The ketoses usually contain primary alcohols at each end of the carbon chain, a ketone group, and a varying number of carbon atoms with secondary alcohols attached. Two common monosaccharides, D-glucose and L-fructose, are examples of aldoses and ketoses respectively (Figure 2). In the Fischer projections of these molecules, the orientation of the hydroxyl at the bottom-most stereocenter determines the D and L notations. In the glucose molecule, the hydroxyl is positioned to the right of the carbon chain, giving it the D configuration; in the fructose molecule, the hydroxyl is positioned to the left of the carbon chain, giving it the L configuration.

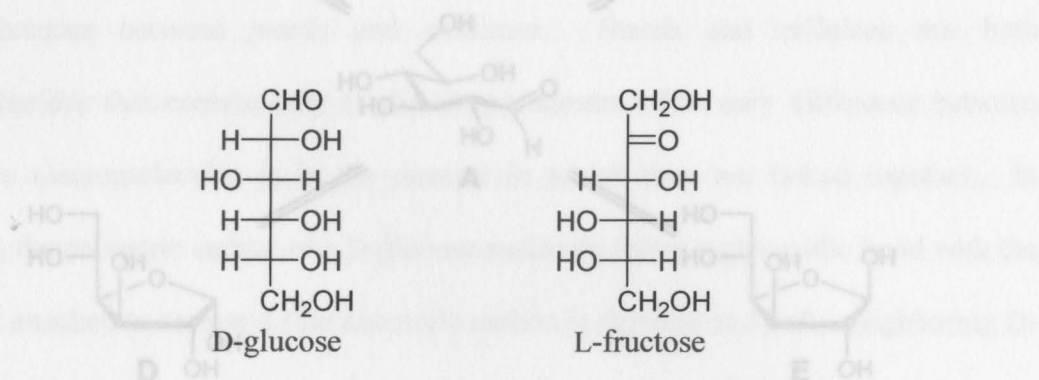


Figure 2: Examples of a six-carbon aldose and ketose.

D-Glucose is one of many molecules classified as a hexose. Hexoses are six carbon sugars that can exist in three overall forms. The least stable of the three forms is known as the *aldehydo*, or linear acyclic, form (Figure 3: A). The drive to form a more stable molecule causes a hydroxyl group on the carbon chain to react with the carbonyl carbon of the exposed aldehyde or ketone on that same chain to yield a hemiacetal or hemiketal cyclic product. This ring-closing reaction results in the formation of either a

five-membered ring denoted as a furanose (Figure 3: **D**, **E**), or a six-membered ring denoted as a pyranose (Figure 3: **B**, **C**).

The cyclic sugar can adopt two configurations for the hydroxyl at the anomeric carbon, or the carbon that was part of the carbonyl. If the anomeric hydroxyl is oriented below the plane of the ring, it is denoted as being α (Figure 3: **B**, **D**). If the hydroxyl is oriented above the plane of the ring, it is denoted as being β (Figure 3: **C**, **E**).

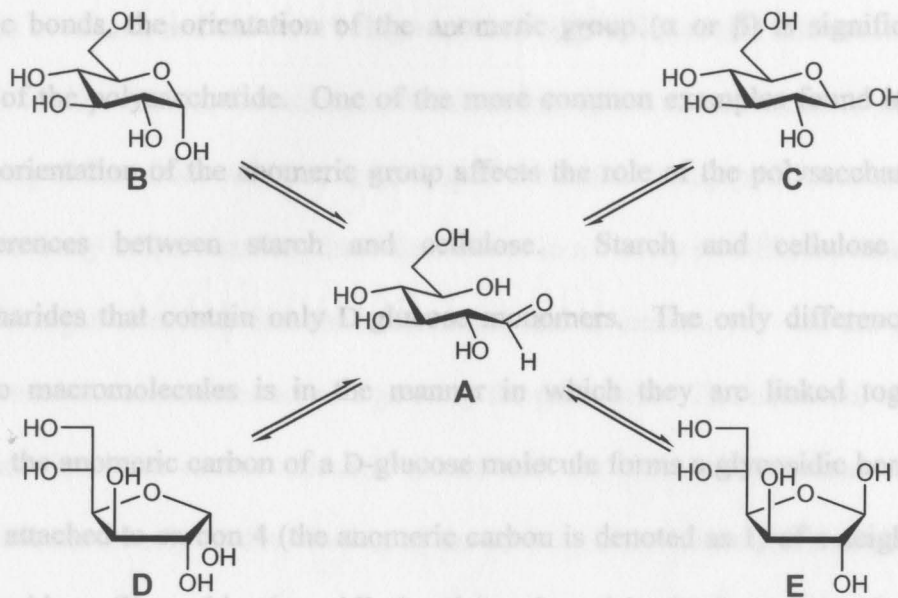


Figure 3: Five forms of D-glucose.

In their pyranose forms, carbohydrates adopt a chair conformation to minimize strain between groups on the tetrahedral carbon atoms. The most stable chair conformation is one in which the larger of the substituents are located in equatorial positions. This limits 1,3-diaxial interactions between axial substituents. Interestingly, β -D-glucose (Figure 3: **C**) is the most abundant monosaccharide found in nature,³ and is the only sugar to have all of its hydroxyl groups situated in the equatorial position simultaneously.

Monosaccharides are able to undergo condensation with other monosaccharides to form long polymers called polysaccharides. To form these polysaccharides, the anomeric group of one sugar condenses with a hydroxyl from another sugar and loses a molecule of water. This bond between the anomeric carbon and the hydroxyl is denoted as a *glycosidic* bond. Considering the number of hydroxyl groups on a sugar that can form a glycosidic bond, one can imagine the different possibilities in which two monosaccharides may be linked. Along with the different alcohols that can form glycosidic bonds, the orientation of the anomeric group (α or β) is significant to the function of the polysaccharide. One of the more common examples found in nature of how the orientation of the anomeric group affects the role of the polysaccharide lies in the differences between starch and cellulose. Starch and cellulose are both polysaccharides that contain only D-glucose monomers. The only difference between these two macromolecules is in the manner in which they are linked together. In cellulose, the anomeric carbon of a D-glucose molecule forms a glycosidic bond with the hydroxyl attached to carbon 4 (the anomeric carbon is denoted as 1) of a neighboring D-glucose residue. Since this glycosidic bond is oriented in the β configuration between carbons 1 and 4, it gets denoted as a $\beta(1\rightarrow4)$ linkage. Starch, on the other hand, employs an $\alpha(1\rightarrow4)$ linkage between the molecules of D-glucose, and differs from cellulose in only the anomeric orientation (Figure 4). This slight difference greatly affects the biochemical properties they possess; starch can be digested by humans, whereas cellulose cannot.

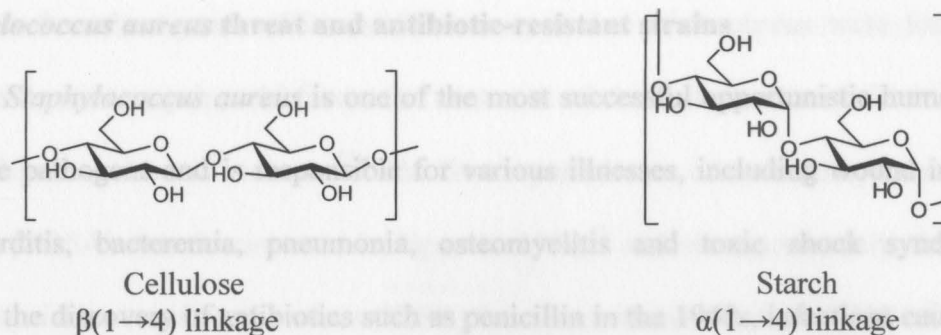


Figure 4: Differences in starch and cellulose linkages.

Carbohydrate analogues, or carbohydrates that have different functionalities, are ubiquitous in nature, and are now being explored as antibiotics and anti-tumor agents as stated previously. Chitin, for example, which makes up the exoskeletons of shellfish and insects, only differs from cellulose in having an acetamido group positioned at carbon 2.⁴ The human body utilizes carbohydrate derivatives in a variety of different functions such as cell and organ structure, cell communication, and in immunity.⁵ On the other hand, carbohydrates can sometimes act as a gateway for pathogens. The influenza virus, the *H. pylori* bacterium that causes stomach ulcers, and the parasitic protozoan that causes Chagas' disease all rely on the binding of the carbohydrate derivative, sialic acid, to the lining of the stomach to absorb into the body. The body counteracts this in infancy, when the stomach is exposed to human milk. Human milk contains sialic acid-containing compounds that the pathogens bind to before interacting with the lining of the stomach.⁶ For this study, we will be focusing on bacteria that utilize carbohydrates to their

Figure 5: Increase in methicillin-resistant strains of *Staphylococcus aureus* in hospitals (filled symbols) and the community (open symbols).¹⁰

The problem of antibiotic resistance in *S. aureus* continued to expand in the early 1990s with the introduction and widespread use of the antibiotic vancomycin to combat the growing number of MRSA cases.¹¹ As was the case with penicillin and methicillin,

***Staphylococcus aureus* threat and antibiotic-resistant strains**

Staphylococcus aureus is one of the most successful opportunistic human Gram-positive pathogens and is responsible for various illnesses, including wound infections, endocarditis, bacteremia, pneumonia, osteomyelitis and toxic shock syndrome.^{7,8,9} Before the discovery of antibiotics such as penicillin in the 1940s, infections caused by *S. aureus* were usually fatal. However, within just four years of its introduction, the first case of penicillin-resistant strains of *S. aureus* was discovered, and within six years, 25% of hospital strains of *S. aureus* were resistant to penicillin.¹⁰

The emergence of penicillin-resistant strains of *S. aureus* caused the rise in use of a closely related type of antibiotic, methicillin. Methicillin-resistant strains of *S. aureus* (MRSA) appeared shortly after its introduction into the medical field, and alarmingly, have risen rapidly (Figure 5) throughout the world.

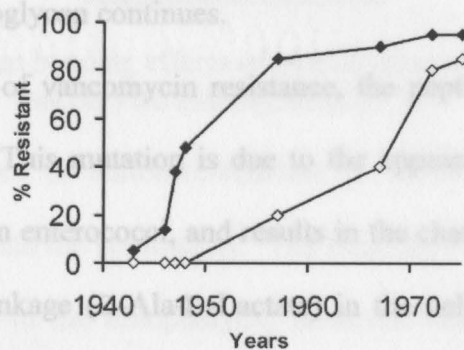


Figure 5: Increase in methicillin-resistant strains of *Staphylococcus aureus* in hospitals (closed symbols) and the community (open symbols).¹⁰

The problem of antibiotic resistance in *S. aureus* continued to expand in the early 1990s with the introduction and widespread use of the antibiotic vancomycin to combat the growing number of MRSA cases.¹¹ As was the case with penicillin and methicillin,

within a few short years of its establishment, strains of *S. aureus* were found to be resistant to vancomycin, which was the treatment of choice for serious infections caused by antibiotic-resistant *S. aureus*.¹² The first reported case of a vancomycin-resistant *S. aureus* (VRSA) was documented in Japan in 1996,¹³ and more commonly, 21 cases of vancomycin-intermediate *S. aureus* (VISA) have been documented as of 2004.¹⁴

The mechanism of resistance to vancomycin by Gram-positive bacteria has been studied extensively. As of 2006, two methods of resistance have been shown prevalent in *S. aureus*; thickening of the cell wall and transferal of the *vanaA* gene from enterococci.^{15,16,17} Thickening of the cell wall is a common feature in VISA and is not directly responsible for vancomycin resistance. Instead, the diffusion coefficient of vancomycin through the cell wall is diminished upon the binding of the antibiotic to the peptidoglycan layers of the cell wall.¹⁷ Essentially, the binding of vancomycin to the outer cell wall 'clogs' the further diffusion of the molecule into the cell cytoplasm, and production of nascent peptidoglycan continues.

In the second model of vancomycin resistance, the peptidoglycan precursors of the cell wall are modified. This mutation is due to the appearance of the *vanaA* gene, which can be transferred from enterococci, and results in the change of an amide linkage (D-Ala-D-Ala) to an ester linkage (D-Ala-D-Lactate) in the cell wall precursors. The change induces a lone-pair repulsion effect between the oxygen of an amide in vancomycin and the modified ester in the peptidoglycan subunit giving rise to a 1000-fold reduction in binding affinity of vancomycin to the cell wall (Figure 6).¹⁸ This pathway is also under study in order to contend with the effects of the modification of cell wall subunits. It has been shown that when the amide bond in vancomycin, the one

that contributes to the lone-pair repulsion, is replaced with a methylene (CH₂), a 100-fold in binding affinity is regained.¹⁸

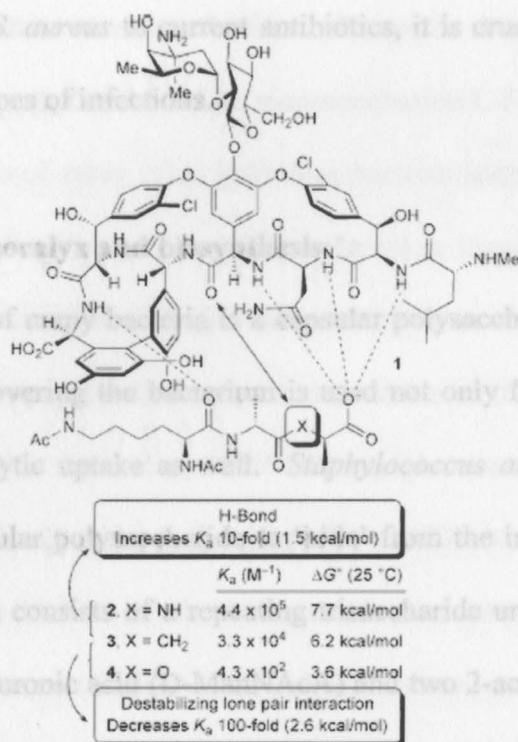


Figure 6: Hydrogen bonding effects of modification of cell wall subunits to vancomycin binding affinity.

Adding to the menace of antibiotic-resistant *S. aureus* is the spread of the infections from the hospital into the community. The majority of humans carry colonies of *S. aureus* on the skin or in the nasopharynx; however, these colonies are usually asymptomatic and do not result in infection.¹⁰ As previously shown in Figure 5, the rates of MRSA's in the community have risen over the past few decades. Community-associated infections usually result from close contact with a person who was recently hospitalized. In recent years, however, these infections have appeared in people who have not been recently hospitalized and have not displayed the typical risk factors for

acquiring such an infection.¹⁰ Further studies show that the spread of the life-threatening disease necrotizing fasciitis, or “flesh-eating disease,” is due to community-associated MRSA.¹⁹ With the combined potential danger of community-associated infections, and the growing resistances of *S. aureus* to current antibiotics, it is crucial to develop novel therapies to combat these types of infections.

Staphylococcus aureus glycocalyx and biosynthesis

A common feature of many bacteria is a capsular polysaccharide, or glycocalyx. This carbohydrate ‘shell’ covering the bacterium is used not only for cell adhesion, but for protection from phagocytic uptake as well. *Staphylococcus aureus* is one type of bacteria that utilizes a capsular polysaccharide to ‘hide’ from the immune system. The glycocalyx in this organism consists of a repeating trisaccharide unit which contains 2-acetamido-2-deoxy-D-mannuronic acid (D-ManNAcA) and two 2-acetamido-2,6-dideoxy galactose residues with both D- and L- configurations (D- and L-FucNAc).⁸ Roughly 80% of all clinical strains of *S. aureus* have glycocalyx type 5 or 8.⁷ Types 5 and 8 are both composed of the aforementioned monosaccharides, but differ only in the linkages between them (Figure 7).

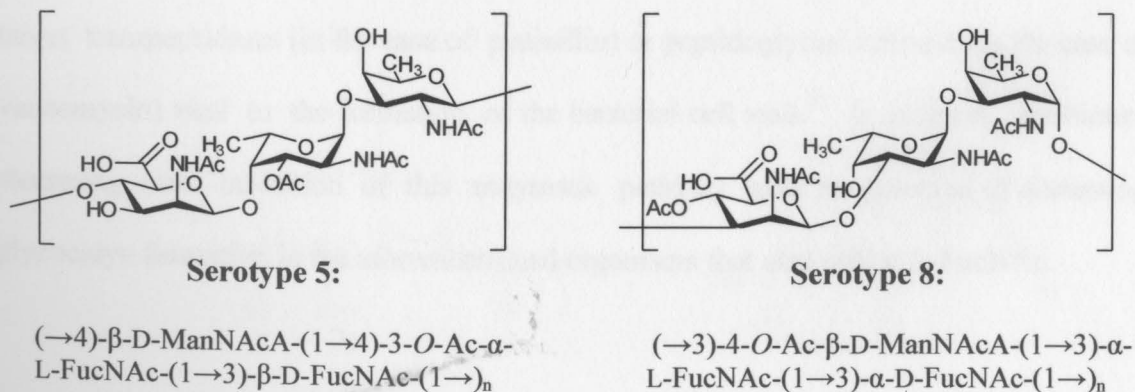
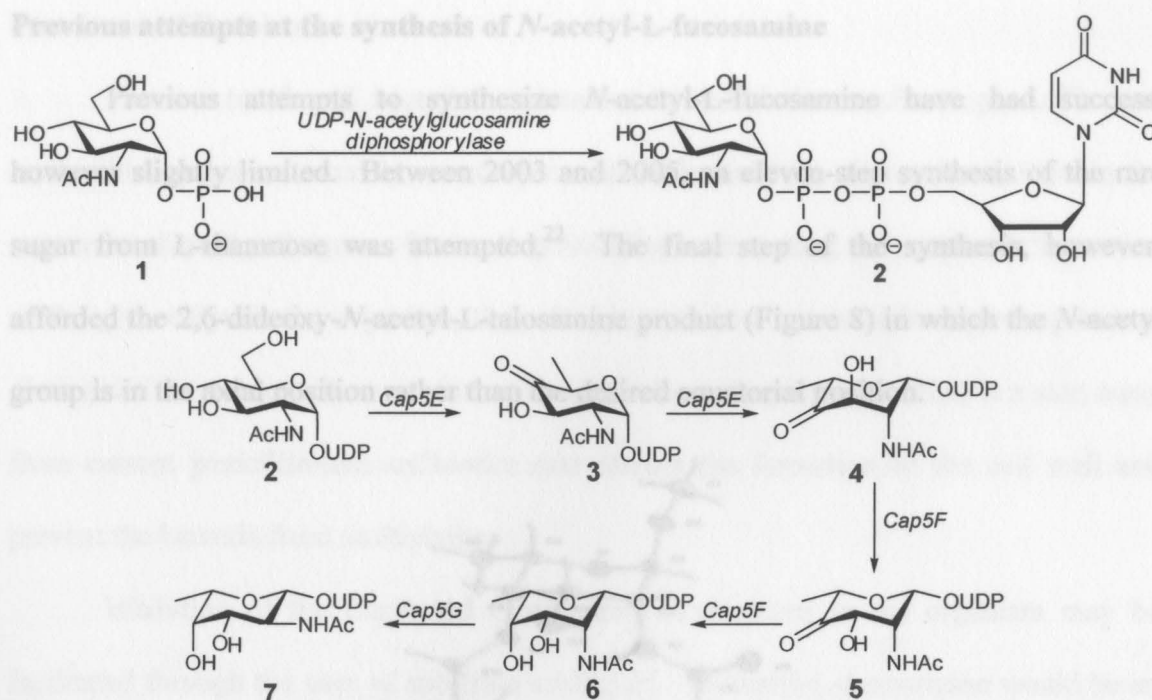


Figure 7: *S. aureus* glycocalyx types 5 and 8.

Biosynthesis of each monosaccharide in the glycocalyx begins with a common starting material, namely, *N*-acetyl-D-glucosamine-1-phosphate (GlcNAc-1-phosphate). In a series of enzymatic reactions, GlcNAc-1-phosphate is converted into UDP-activated analogues of each of the three monosaccharides. Enzymes then condense the three monomeric units to yield the glycocalyx. The monosaccharide L-FucNAc is common in the capsular polysaccharides of many other infectious bacteria such as *P. aeruginosa*, *E. coli*, *S. pneumoniae*, and *B. fragilis*, but is not found elsewhere in nature.²⁰

Experimental evidence by Kneidinger and associates, as well as Mulrooney and coworkers, propose a four-enzyme pathway in the conversion of D-GlcNAc-1-phosphate to UDP-L-FucNAc. In the first step, *UDP-N-acetylglucosamine diphosphorylase* catalyzes the conversion of D-GlcNAc-1-phosphate (1) to UDP-*N*-acetyl-D-glucosamine (UDP-GlcNAc) (2). UDP-GlcNAc is then converted to a keto-deoxy sugar in two reactions catalyzed by the enzyme *Cap5E*; a 4,6-dehydration and an epimerization at C-5 (4). This keto-deoxy sugar is subsequently reduced at C-4 and epimerized at C-3 to give UDP-2-acetamido-2,6-dideoxy-L-talose (UDP-PneNAc) (6) by the enzyme *Cap5F*. In the sixth and final step in the pathway, the enzyme *Cap5G* inverts the stereochemistry about C-2 of UDP-PneNAc to yield the final product, UDP-L-FucNAc (7).^{7,20}



Kneidinger and coworkers also found that inactivation of *Cap5F* or *Cap5G* genes resulted in complete prevention of the capsular polysaccharide production in *S. aureus*.⁷ Using this enzymatic evidence, one can theorize that a glycomimetic inhibitor of one of these enzymes could result in disruption of UDP-L-FucNAc synthesis, and possibly, disruption of the glycocalyx formation. This approach to possible antibiotics is novel in the sense that current antibiotics used to treat *S. aureus* target transpeptidases (in the case of penicillin) or peptidoglycan subunits (in the case of vancomycin) vital to the formation of the bacterial cell wall.²¹ In addition, antibiotics stemming from inhibition of this enzymatic pathway have the potential of disrupting glycocalyx formation in the aforementioned organisms that also utilize L-FucNAc.

Figure 9: X-Ray crystal structures of 2,6-dideoxy-*N*-acetyl-L-fucosamine (left) and its protected 2-azidodeoxy derivative (right).

Previous attempts at the synthesis of *N*-acetyl-L-fucosamine

Previous attempts to synthesize *N*-acetyl-L-fucosamine have had success, however slightly limited. Between 2003 and 2005, an eleven-step synthesis of the rare sugar from L-rhamnose was attempted.²² The final step of the synthesis, however, afforded the 2,6-dideoxy-*N*-acetyl-L-talosamine product (Figure 8) in which the *N*-acetyl group is in the axial position rather than the desired equatorial position.

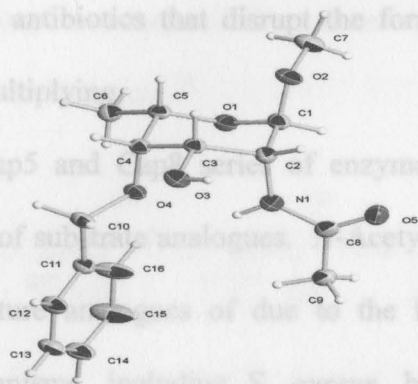


Figure 8: X-Ray crystal structure of protected 2,6-dideoxy-*N*-acetyl-L-talosamine.

N-Acetyl-L-fucosamine has been successfully synthesized utilizing a seven-step pathway from L-fucose. Although this synthesis gives the desired product as well as the 2-azidodeoxy derivative (Figure 9), the starting material L-fucose is expensive (100 g = \$1500) and the final product has only been obtained in a 13.7% total yield.²³

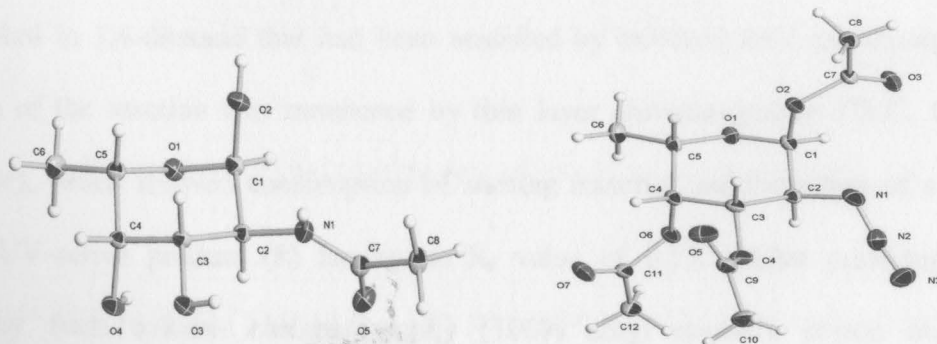


Figure 9: X-Ray crystal structures of 2,6-dideoxy-*N*-acetyl-L-fucosamine (left) and its protected 2-azidodeoxy derivative (right).

Statement of Problem

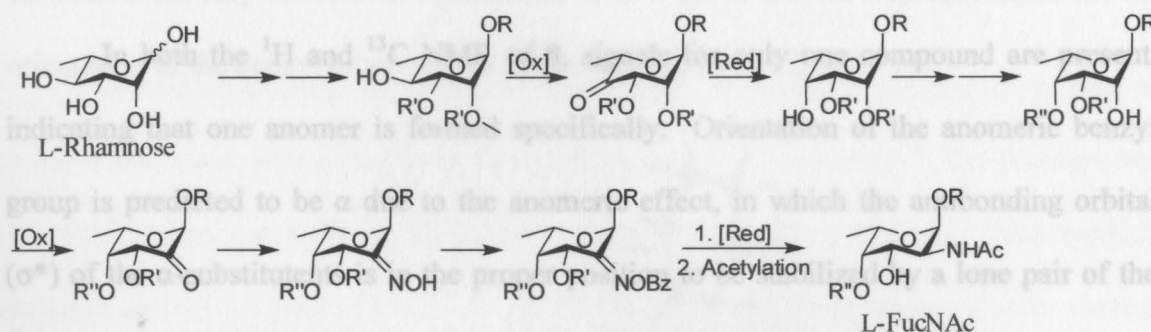
Current trends of bacterial resistance to antibiotics such as penicillin and methicillin, and more recently vancomycin, drive the need for alternative options in the treatment of such pathogens. One such possibility is disrupting the enzymatic formation of the glycocalyx in the organism, thus allowing the host's natural immune response to distinguish the bacteria from normal cells and induce phagocytosis. This is a step away from current penicillin-like antibiotics that disrupt the formation of the cell wall and prevent the bacteria from multiplying.

Inhibition of the Cap5 and Cap8 series of enzymes in the organism may be facilitated through the uses of substrate analogues. *N*-Acetyl-L-fucosamine would be an ideal substrate to manufacture analogues of due to the fact that it is found in the glycocalyx of several organisms, including *S. aureus*, but is not found in human biochemistry. Being that this sugar is only found in bacteria, it would be difficult to isolate large quantities of it to use as a starting material in the synthesis of analogues. Therefore, it is necessary to develop a scalable and cost-effective synthesis of *N*-acetyl-L-fucosamine to further study the effects of inhibition of the glycocalyx formation in *S. aureus* and other pathogens.

Results and Discussion

1. Attempted synthesis of L-FucNAc from L-rhamnose via oxidation/reduction/inversion of the C-2 and C-4 stereocenters

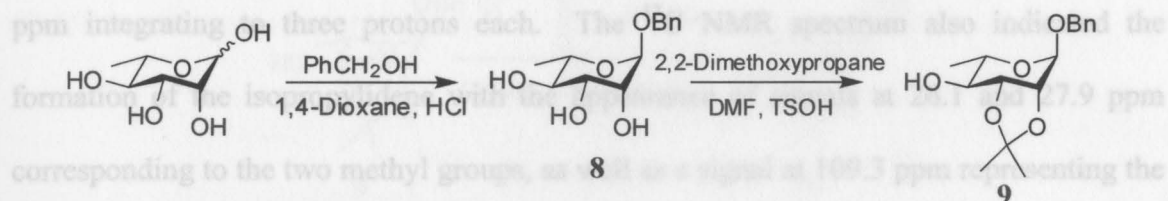
In the first of two attempted conversions of L-rhamnose to L-FucNAc, the C-2 and C-4 stereocenters must be individually isolated and inverted through the use of oxidations and selective reductions, as well as the oxygen at C-2 being replaced by nitrogen (Scheme 2). The C-4 hydroxyl was targeted first, since a protection strategy to isolate that hydroxyl was known in the literature.²⁴



Scheme 2: First synthetic strategy from L-rhamnose to a protected L-FucNAc.

Isolation of the hydroxyl at C-4 was achieved in two steps starting from L-rhamnose (Scheme 3). In the first step of the synthesis, L-rhamnose was reacted with benzyl alcohol in 1,4-dioxane that had been acidified by bubbling HCl gas through it. Completion of the reaction was monitored by thin layer chromatography (TLC, 100% ethyl acetate), which showed consumption of starting material and formation of a new less polar UV-active product (**8**) having an R_f value of 0.15. After purifying the glycoside by flash column chromatography (100% ethyl acetate), proton nuclear magnetic resonance (^1H NMR) showed the appearance of a 5H multiplet at 7.32 ppm

corresponding to the phenyl ring hydrogens as well as the two doublets at 4.40 and 4.59 ppm representing the diastereotopic hydrogens of the newly added benzyl group. The four signals in the carbon NMR spectrum (^{13}C NMR) between 127.7 and 136.9 ppm further indicate the formation of the benzyl glycoside **8** in a 68% yield.



Scheme 3: Isolation of the C-4 hydroxyl from L-rhamnose.

In both the ^1H and ^{13}C NMR of **8**, signals for only one compound are present, indicating that one anomer is formed specifically. Orientation of the anomeric benzyl group is predicted to be α due to the anomeric effect, in which the antibonding orbital (σ^*) of the α -substituents is in the proper position to be stabilized by a lone pair of the ring oxygen (Figure 10). This interaction allows the α -anomer to be the thermodynamically favored product of this reversible glycosylation reaction, since the β -anomer has no σ^* orbital overlap.

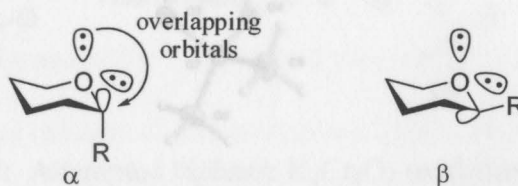


Figure 11: X-Ray crystal structure of **9**.

Figure 10: Orbital overlapping effects on α - and β -anomers.

After isolation of C-4, attempts were made to oxidize the secondary hydroxyl to a ketone under neutral or basic conditions to avoid cleavage of the newly formed acid-sensitive isopropylidene group. First, the oxidation was performed under typical Swern

hours, TLC (2:1 hexanes:ethyl acetate) showed formation of a new less polar spot having an R_f of 0.19. Removal of the solvent afforded **9** as white crystals in an 83% yield. Since there is no C-C bond rotation in the isopropylidene group, the two chemically equivalent methyl groups show as individual peaks in the ^1H NMR spectrum of **9** at 1.25 and 1.38 ppm integrating to three protons each. The ^{13}C NMR spectrum also indicated the formation of the isopropylidene with the appearance of signals at 26.1 and 27.9 ppm corresponding to the two methyl groups, as well as a signal at 109.3 ppm representing the acetal carbon. An X-ray crystal structure was obtained from the product, which confirmed not only the selective protection of C-2 and C-3 as an isopropylidene, but the orientation of the benzyl group as α at the anomeric position (Figure 11).

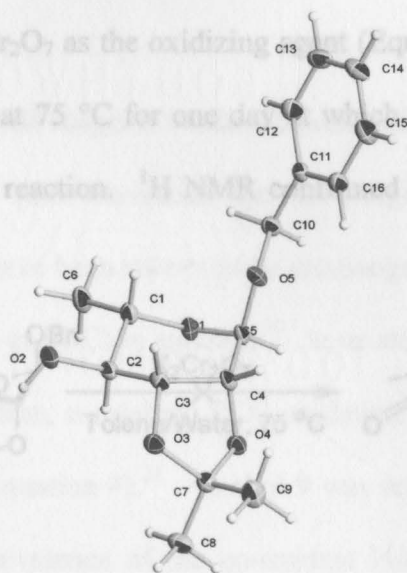
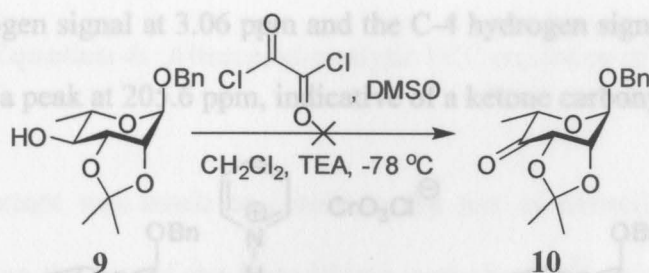


Figure 11: X-Ray crystal structure of **9**.

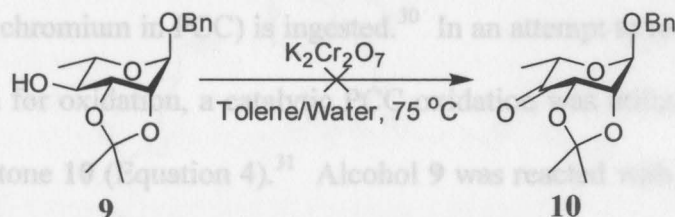
After isolation of C-4, attempts were made to oxidize the secondary hydroxyl to a ketone under neutral or basic conditions to avoid cleavage of the newly formed acid-sensitive isopropylidene group. First, the oxidation was performed under typical Swern

conditions^{25,26,27} (Equation 1) using oxalyl chloride, dimethyl sulfoxide and triethyl amine. No sign of reaction was found by TLC (2:1 hexanes:ethyl acetate) after stirring for two days and ¹H NMR confirmed the presence of only starting material **9**.



Equation 1: Attempted Swern oxidation of **9**.

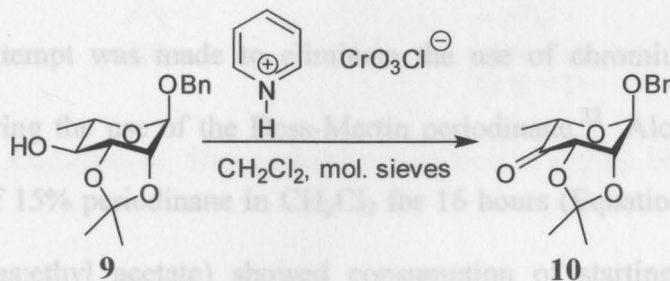
A second attempt to oxidize **9** was carried out using a two-phase reaction in toluene and water with $K_2Cr_2O_7$ as the oxidizing agent (Equation 2).²⁸ The reaction was stirred vigorously at reflux at 75 °C for one day at which time TLC (2:1 hexanes:ethyl acetate) showed no sign of reaction. ¹H NMR confirmed the presence of only starting material **9**. These reagents have been shown to be carcinogenic when chromium(VI) (the



Equation 2: Attempted biphasic $K_2Cr_2O_7$ oxidation of **9**.

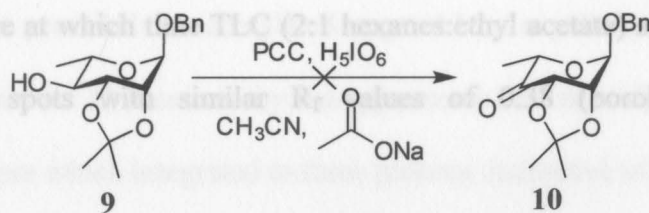
The oxidation of **9** to ketone **10** was successfully carried out using a five molar equivalence of pyridinium chlorochromate (PCC) in CH_2Cl_2 with 4Å molecular sieves over three days (Equation 3).²⁹ After the third day, TLC (2:1 hexanes:ethyl acetate) showed the consumption of the starting material and the formation of a less polar spot

with an R_f of 0.55. After passing the crude reaction mixture through a column of silica gel and subsequent washing with a 1:1 hexanes:diethyl ether solution, the solvent was removed to afford **10** as a clear oil in 86% yield. ^1H NMR showed the disappearance of the hydroxyl hydrogen signal at 3.06 ppm and the C-4 hydrogen signal at 5.21 ppm. ^{13}C NMR also showed a peak at 205.6 ppm, indicative of a ketone carbonyl.



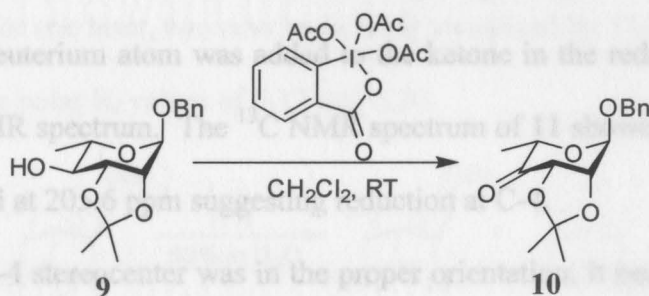
Equation 3: Formation of ketone **10** via PCC oxidation.

While chromium-based reagents readily oxidize secondary alcohols to ketones, the health risks for using such chemicals far out-weighs the convenience of their reactivity. These reagents have been shown to be carcinogenic when chromium(VI) (the oxidation state of chromium in PCC) is ingested.³⁰ In an attempt to reduce the amount of chromium needed for oxidation, a catalytic PCC oxidation was utilized in the oxidation of alcohol **9** to ketone **10** (Equation 4).³¹ Alcohol **9** was reacted with PCC (2 mol %) in acetonitrile with a 1.05 equivalence of the co-oxidant H₅IO₆ and sodium acetate as a buffer, however after two days of stirring at room temperature, no reaction was seen by TLC (2:1 hexanes:ethyl acetate). ^1H NMR confirmed that no reaction had take place, showing only the spectrum of the starting alcohol **9**.



Equation 4: Attempted catalytic PCC oxidation of **9**.

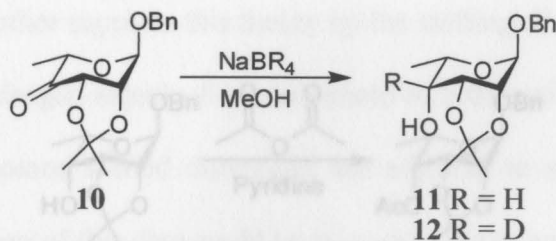
A final attempt was made to eliminate the use of chromium-based oxidizing agents by employing the use of the Dess-Martin periodinane.³² Alcohol **9** was reacted with a solution of 15% periodinane in CH_2Cl_2 for 16 hours (Equation 5), at which time TLC (2:1 hexanes:ethyl acetate) showed consumption of starting material and the formation of a new less polar spot having an R_f of 0.80. After basic hydrolysis of the formed hydroxyl group at 2.43 and 2.30 ppm for **11** and **12** respectively, Alcohol **11** also excess periodinane to the water-soluble 2-iodosobenzoate and removal of solvent, ^1H NMR remained consistent with that of the product of the PCC oxidation indicating that different from that of the alcohol **9** indicating that the stereochemistry at the C-4 position ketone **10** was formed.



Equation 5: Dess-Martin oxidation of **9** to ketone **10**.

Ketone **10** was then reduced using two reagents, sodium borohydride (NaBH_4) and sodium borodeuteride (NaBD_4 , Equation 5). In both cases, the ketone was dissolved in methanol and an excess of reducing agent was added and allowed to stir for two hours formation of a new less polar spot with an R_f of 0.51. Isolation of the product after

at room temperature at which time TLC (2:1 hexanes:ethyl acetate) showed formation of new more polar spots with similar R_f values of 0.38 (borohydride) and 0.37 (borodeuteride).



Equation 6: Stereoselective reduction of ketone **10**.

^1H NMR analysis of the products showed similar broad ^1H signals for the newly formed hydroxyl group at 2.43 and 2.25 ppm for **11** and **12** respectively. Alcohol **11** also showed a new doublet at 3.55 ppm having a coupling constant of 5.13 Hz, significantly different from that of the alcohol **9** indicating that the stereochemistry at the C-4 position had been inverted. Alcohol **12** showed no new hydrogen signal corresponding to C-4 however since a deuterium atom was added to the ketone in the reduction and does not show in the ^1H NMR spectrum. The ^{13}C NMR spectrum of **11** showed the disappearance of the ketone signal at 205.6 ppm suggesting reduction at C-4.

After the C-4 stereocenter was in the proper orientation, it needed to be protected in order to be able to further manipulate the sugar without compromising the inverted hydroxyl. The protecting group also had to be acid-stable, since acid-catalyzed removal of the isopropylidene group was necessary. In the first attempt at such protection, **11** was reacted with acetic anhydride in pyridine (Equation 7) for two days, at which time TLC (2:1 hexanes:ethyl acetate) showed the consumption of starting material and the formation of a new less polar spot with an R_f of 0.51. Isolation of the product after